2018

Role Of Bed Design Characteristics On The Effective Thermal Conductivity Of A Structured Adsorbent

Pravin Bosco Charles Antony Amalraj
University of South Carolina

ROLE OF BED DESIGN CHARACTERISTICS ON THE EFFECTIVE THERMAL CONDUCTIVITY OF A STRUCTURED ADSORBENT

by

Pravin Bosco Charles Antony Amalraj

Bachelor of Technology
Anna University, 2016

Submitted in Partial Fulfillment of the Requirements

For the Degree of Master of Science in

Chemical Engineering

College of Engineering and Computing

University of South Carolina

2018

Accepted by:

James A. Ritter, Director of Thesis

Armin D. Ebner, Reader

John R. Monnier, Reader

John W. Weidner, Reader

Cheryl L. Addy, Vice Provost and Dean of the Graduate School

DEDICATION

To my dearest parents and family without whose support and constant encouragement, none of this would have been possible. I would like to thank them for all the love and sacrifice.

ACKNOWLEDGEMENTS

"For it is by God's grace that you have been saved through faith. It is not the result of your own efforts, but God's gift, so that no one can boast about it." – Ephesians 2:8-9

I would like to express my deepest gratitude to my advisor Dr. James Ritter for believing in me, accepting me into his research group and for being a great mentor. It was an amazing learning experience to work with Dr. Armin Ebner, who patiently taught me and constantly pushed me to give my best effort. Their support and guidance is invaluable to me for the successful completion of my thesis. I would like to thank Dr. Marjorie Nicholson, and all of my fellow group members who have been kind and helpful to me throughout. I would like to express my sincere appreciation to my committee members Dr. John Monnier and Dr. John Weidner, for their time. Finally, I would like to thank all my beloved friends who have made this journey a memorable one for me.

ABSTRACT

This work evaluates the role of different design variables on the effective thermal conduction of a structured adsorbent bed for its possible application in a temperature swing adsorption (TSA) process. The structured adsorbent bed is represented by eight parallel layers of intercalated smooth and corrugated foils of a metal support coated with 13X zeolite resulting in the formation of parallel triangular channels. The variables investigated include the thickness of the adsorbent coating, thickness of the metal, nature of contacts between smooth and corrugated foils, type of metal, presence and magnitude of an air gap between the foils, difference in alignment of the metal foil, difference in the coating methodology and effect of different void gases.

The effective thermal conductivity evaluated in this work was that obtained by modelling the heat transfer through the bed in the direction perpendicular to the foils and at steady state. This two-dimensional model representing the cross section of the bed was developed in COMSOL Multiphysics. The specific heat power at one end of the bed was defined and fixed at 500 W/m^2 while the temperature of the other end was fixed at 293.15 K. The sides of the structured bed were thermally insulated. The pressure of the void gas within the channels was fixed at 1 atm, with the gas density freely adjusting with temperature and according to the ideal gas law. Depending on the design parameters the width of the bed cross section varied between 1.247 and 1.827 cm while the depth of the bed cross section was identical in all cases and equal to 0.32 cm.

The results showed that the effective thermal conductivity in the direction perpendicular to the foils is significantly impacted by the conductivity of the metal, if the foils were in direct contact either via imbedding or via direct metal to metal point contacts. Under this condition, the thermal conductivity depended strongly on the conductivity of metal, and weakly on the conductivity of gas medium and all other design properties. For these metal foils in air, the thermal conductivities varied between 0.561 and 0.629 W/m/K, when the metal was stainless steel, whereas for aluminum, a value of 6.66 W/m/K was obtained. In contrast, when the foils were separated either by air gaps or by a 13X coating, the effective thermal conductivity was significantly reduced, and it depended strongly on the conductivity of the gas medium and weakly on the metal conductivity and all other design properties. For example, in air and whether the metal was stainless steel 304 or aluminum, the thermal conductivities were always around 0.090 and 0.125 W/m/K.

TABLE OF CONTENTS

LIST OF TABLES

LIST OF FIGURES

LIST OF SYMBOLS

D_{bed}	Depth of the bed under study, cm
k_{eff}	Effective thermal conductivity, W/m/K
q	Heat flux density, W/m^2
T	Temperature, K
$T_{z=0}$	Temperature at the left boundary in the bed, K
$\bar{T}_{z=w}$	Average temperature at the right boundary in the bed, K
w	Width of the cross section of the bed, cm
δ_a	Thickness of the adsorbent coating, μm
δ_g	The magnitude of the gap between metal foils, μm
δ_m	Thickness of the metal, μm
ρ	Density, kg/m^3

LIST OF ABBREVIATION

Al..... Aluminum

CFD..... Computational Fluid Dynamics

PSA .....Pressure Swing Adsorption

SS 304 ..... Stainless Steel AISI 304

TSA .....Temperature Swing Adsorption

3D..... Three-dimensional

2D..... Two-dimensional

CHAPTER 1

INTRODUCTION

Gas separation and purification is a constant emerging field with tremendous scope of process improvement and intensification. Cyclic adsorption technologies, mainly pressure swing adsorption (PSA) and temperature swing adsorption (TSA) are some of the most widely used methods for selective removal of species from a gas mixture [1]. The various challenges constantly faced by these processes are maintaining a good working capacity per cycle with high feed throughputs. In this, handling higher velocities with lower pressure drops while protecting the integrity of the adsorbent and mass transfer properties of the adsorbent is key to a cost-effective design [2]. Traditionally, the type of adsorbent materials used in adsorptive process are in the form of beads or granules that play a significant role in imposing limitations to bed velocities, especially in large scale systems [2] [3].

In order to overcome these drawbacks, efforts have been made in the past few decades to progress towards the development of new novel adsorbent structures. These materials are not subject to the mechanical degradation that results from high velocities and in some in cases, they can additionally provide low pressure drops. Fabrics [3]-[8], foams [9]-[10], laminate sheets [11]-[14], and monoliths [15]-[29] have become the emerging technology in adsorptive gas separation, with some of them reaching the stage of commercialization [15-21]. Of special interest are monolith structured adsorbents where

the active material is added to an inert support via coating by impregnation approaches such as dip-coating, slip-coating, wash-coating and slurry coating [30]-[34]. In all these cases, limitations upon mass transport of gases due to adsorbent size are eliminated and consequently, for systems that are naturally macropore limited, the low effective bed bulk densities typical of structured adsorbents become compensated by inherent faster regeneration kinetics.

Because of their faster kinetics and the ability to handle high velocities to cope with reduced cycle times, structured adsorbents seem naturally more suitable to PSA systems, as TSA processes are significantly limited by slow cooling and heating due principally by the low thermal conductivity of adsorbents. For this reason, the commercialization of structured adsorbent toward TSA has more geared from the practical aspects of structured adsorbents, as is with the case of commercially stablished rotary desiccant wheels [35-37]. In general, the naturally slower cycle times have essentially limited TSA to guard processing and the removal of heavy gases where the utilization of pelletized systems offering larger bulk densities has been to date more justified.

There has been some research focused on possibilities to improve on cycle times of TSA. In this regard, efforts have been mostly focused on improving the speed of heating of beds by exploiting the electric conductivity of graphitic based structured adsorbents [22-29]. However, these processes are still limited by slow cooling and cannot be applied to process where zeolites or other non-carbon based materials present thermodynamic advantage. To date, no research efforts are devoted to address the low thermal conductivity of beds.

The advent of structured sorbents or catalysts the form of films coated on metallic structures [21] may open the possibility for new improvements toward reducing cycle times in TSA. Metallic supports can be good conveyors of heat that may have a significant impact in both heating and cooling in beds that may only require an external jacket to such effect. The present work evaluates different aspects of coated adsorbents of metallic structures to evaluate the potential benefits of using these materials in TSA processes. The metallic supports consist of an alternate combination of smooth and corrugated foils forming triangular channels. With the aid of Comsol^{TM}, computational studies were carried out to explore and understand the thermal response of these novel structured adsorbents. The thermal response was evaluated in terms of the effective thermal conductivity of the modelled material by evaluating different parameters that include the thickness of the adsorbent coating, the thickness of the metal, the type of metal, loose or imbedded corners at the point of contact between corrugated and smooth foils, the presence and magnitude of air gap between the foils, coating on just one or both sides of the foils, and the role of the gas. All the runs gives us valuable information for continuing further studies in this area, which can be extended further experimentally in the future as well.

CHAPTER 2

MATHEMATICAL MODEL

Figure 2.1 shows a simplified schematic a two-dimensional control volume utilized in this work depicting a cross section of a structured adsorbent to evaluate its effective thermal conductivity in one given direction, which is akin to the radial thermal conductivity in a cylindrical woundup structured bed constructed by wrapping metal foils around a central rod. The cross section of the structured adsorbent consists of nine smooth foils and eight corrugated foils coated with 13X zeolite and placed in alternating fashion along the width of the cross section forming triangular channels as shown. The cross section is only two-triangle deep. The effective conductivity of interest is that in the direction perpendicular to the surface of the smooth foils, which is the one offering largest resistance to heat transfer due to possible metal discontinuity. To effectively evaluate the thermal conductivity of the adsorbent in that direction, the upper and lower sides of the control volume are assumed thermally insulated, left boundary at a temperature fixed at $T_{z=o}$ = 293.15K, and the right boundary homogeneously receiving a specific power of q = 500 W/m^2. The effective thermal conductivity in the indicated direction is given by:

$$K_{eff} = \frac{w.q}{\bar{T}_{z=w} - T_{z=0}} \quad (1)$$

Where w the width of the cross section of the bed, and $\bar{T}_{z=w}$is the average temperature on the right boundary of the control volume. The problem is simulated with COMSOL Multiphysics 5.2 by resolving the steady state problem

$$\nabla^2 T = 0 \tag{2}$$

With heat transfer continuity at each boundary between two materials that include either the gas medium, the metal frame or the zeolite 13X. The gas medium is assumed to be at one atmosphere with its density freely changing according to the resulting temperature under ideal gas law assumption. Also, its conductivity was assumed to be independent of pressure and given by known values of the gases used at 1 atm. No momentum or mass balance was used.

At the bottom left end, Figure 2.1 also highlights the repeating unit cell of the structure adsorbent. The alternative unit cells investigated in this work are given in Figure 2.2, wherein the foils are assumed either imbedded (2.2.b and 2.2.d) or loosely connected (2.2.a, 2.2.c, 2.2.e and 2.2.f), either with (2.2.c through 2.2.f) and without (2.2.a and 2.2.b) coating; and whether the coating is carried out either pre (2.2.c and 2.2.e) or post (2.2.d, and 2.2.f) assembling the structure. The parameters δ_a, δ_m and δ_g respectively represent the thickness of the adsorbent coating, the thickness of the metal and the gas medium gap between a contiguous smooth and a corrugated foil. The role of having the cells configured in an even or in an uneven fashion (Figure 2.3) was also considered. The values of these parameters, and materials used in this study are given in tables Table 2.1 and Table 2.2 respectively. The properties of the gases used in simulation was also obtained from reference [38].

CHAPTER 3

RESULTS AND DISCUSSION

Table 3.1 gives a summary of the entire work with the different designs and simulations conditions used as a part of the modelling in the form of 24 different runs. The Table also provides the resulting effective thermal conductivities obtained in each of these runs. All the control volumes are 0.32 cm in depth, with varying width from 1.247 cm (runs [1-4]) to 1.827 cm (run 14), based on the different design criteria. Stainless steel AISI 304 is used as a standard metal framework for most of the design cases, with the variation of using Aluminum for certain cases of study. Air is the gas medium for most of the cases, with helium and CO_2 used for studying the impact of different gas media.

Figure 3.1 shows a comparison of the effective thermal conductivity between two different foil assembly with the difference in the way the SS 304 metal foils of 50 μm thickness are in contact with each other. Both cases have air as the gas medium. The loose contact is the case where the smooth metal foils are in contact with the sharp corners of the corrugated foils when they are rolled together as shown in Figure 2.2.a with a gas medium gap $\delta_g = 0$. The imbedded contact is the case where the foils are rolled together and the sharp corners of the corrugated foils are imbedded into the smooth metal foils as shown in Figure 2.2.b. The results shown corresponds to runs 1 and 2 in Table 3.1. The imbedding tends to increase the surface area of contact between the foils and improves the heat conduction in the system but not significantly. The effective thermal conductivity of the

imbedded system is 0.629 W/m/K, which is very close to the loose contact system with conductivity of 0.575 W/m/K.

Figure 3.2 shows the effect of using different gas media on the effective thermal conductivity of a system with SS 304 having loose contacts between the metal foils of 50 μm thickness. The unit cell used is that of Figure 2.2.a with a gas medium gap $\delta_g = 0$ is selected. The results shown corresponds to runs 1, 3 and 4 in Table 3.1, where helium and carbon dioxide are chosen as gas media for comparison with air. The system having helium gas had an effective thermal conductivity of 0.726 W/m/K, while CO_2 resulted in a value of 0.563 W/m/K, which is similar to that of system with air medium. It is evident from the figure that the effect of the different gas media has a small effect on k_{eff} , when the smooth and the corrugated metal foils are in direct contact with each other.

Figure 3.3 shows the effect of having different gas gaps δ_g between the smooth and the corrugated SS 304 metal foils on the effective thermal conductivity of a system. Metal thickness of 50 μm was chosen for the foils and air is the gas medium. The same unit cell used in Figure 3.2 (i.e., that shown in Figure 2.2.a) is used here with gas gaps of 0 μm, 10 μm, 30 μm and 50 μm are chosen as shown in the runs 1, 5, 6 and 7 in Table 3.1, respectively. The k_{eff} for the three air gaps are 0.119, 0.099 and 0.090 W/m/K respectively. When compared to the loose contact design with no gap, the presence of even 10 μm gap between the foils brings down the k_{eff} value by a massive 80%, whereas increasing the gaps further had a minimal effect on the conductivity.

Figure 3.4 shows the role of different gas media on the effective thermal conductivity of a system with SS 304 having $\delta_g = 10$ μm using again the same unit cell of

Figures 3.2 and 3.3 (i.e., that shown in Figure 2.2.a). The Metal thickness of 50 μm was chosen for the foils and helium and carbon dioxide are chosen. The results shown corresponds to runs 8 and 9 in Table 3.1. The k_{eff} for helium gas was found to be 0.46 W/m/K, and for carbon dioxide it was determined to be 0.085 W/m/K. On comparison, for helium system the conductivity is 4 times than that of the air system, and for the system with carbon dioxide the value is 1.4 times lower than the system containing air. We find the nature of gas media used becomes significant, when there is presence of gaps of at least 10 μm separating the metal foils.

Figure 3.5 shows the role of different gas media on the effective thermal conductivity of a system having 30 μm adsorbent coating on the SS 304 metal foils of thickness 50 μm using loose metal foils with point contacts (δ_g = 0 μm). Figure 2.2.c shows the unit cell considered for this case. The results shown corresponds to runs 10, 11 and 12 in Table 3.1. It was found that the system with helium has an effective thermal conductivity of 0.345 W/m/K which is thrice that of air, and for carbon dioxide system it was 0.087 W/m/K which is 1.3 times lower than that of air system. The fundamental study with different gases again proves how the adsorbent coating separating the metal foils from contact, makes the gas media an important factor on k_{eff} of the bed. The results also show how the existence of adsorbent between the metal foils at the point contacts, also significantly reduces k_{eff} of the bed relative to the case where the metals of the foils are in direct contact (Figures 3.1 and 3.2).

Figure 3.6 shows role of different adsorbent coating thickness δ_a of zeolite 13X and its impact on the effective thermal conductivity of the SS 304 system. The figure

includes the case where the foils are loose with point contact (δ_g = 0 μm) or imbedded. The respective unit cells are that of Figure 2.2c in the case of the loose foils and Figure 2.2.d for the imbedded foils. Metal foils are 50 μm in thickness. The results shown corresponds to runs 10, 13-17 in Table 3.1. When we consider the imbedded design which have been post-assembly coated with adsorbent thickness of 30 μm, 50 μm and 100 μm, the effective thermal conductivity is found to be 0.620, 0.623 and 0.623 W/m/K respectively, and makes it evident that with increasing thickness of adsorbent coating there is a negligible change in conductivity of the imbedded system. In case of the loose contact design, the conductivity of the system with 30 μm, 50 μm and 100 μm is found to be 0.112, 0.107 and 0.101 W/m/K respectively, and increasing thickness decreases the conductivity negligibly. With the two different foil assembly, there is 5.5 to 6 times increase in k_{eff} of imbedded contacts, when compared to the loose contacts for the three δ_a. We find how the contacts between the metal foils makes a signficant impact in our observations, and the thickness of adsorbent coating doesn't have an impact on k_{eff} of the bed.

Figure 3.7 shows the effect of the metal thickness δ_m on the effective thermal conductivity. The same unit cell of Figure 3.5 is used (i.e., that shown in Figure 2.2.c) with the loose metal foils with point contacts (δ_g = 0 μm), using SS 304 as the metal and having 30 μm of adsorbent coated on it. The three metal thickness chosen are 50 μm, 80 μm and 100 μm. The results shown corresponds to runs 10, 18 and 19 in Table 3.1. The results of the k_{eff} value for these cases are 0.112, 0.12, 0.125 W/m/K for the three thickness respectively. The change of metal thickness doesn't affect the k_{eff} of the bed, and the values obtained are very similar to those shown in the previous figure with loose coated

foils with point contact (i.e., runs 10, 13 and 14). This indicates that the adsorbent coating separating the metal of the foils from having direct contact is again reponsible for the low values of k_{eff}.

Figure 3.8 shows the role of having adsorbent coating of 30 μm thickness only on the corrugated SS 304 metal loose foils of 50 μm thickness with point contacts (δ_g = 0 μm) in comparison to the same case but with both foils having an adsorbent coating of 30 μm thickness. The unit cell for this particular case of having coating only in the corrugated foils is that of Figure 2.2.e using air as the gas medium. The results shown corresponds to runs 10 and 20 in Table 3.1. The results of k_{eff} reveals that the effective themal conductivity value is 0.118 W/m/K, which is identical whether coating is either on one or both the metal foils. This is again attributed to the fact that the adsorbent coating separates the metal foils from having direct contact.

Figure 3.9 shows the role of the metal in the foil (aluminum or SS 304) on the effective thermal conductivity of the system. The figures also compares the role of loose foils with point contacts (δ_g = 0 μm) either having or not having the coating of 13X zeolite separating the metal foils from contacting each other. The unit cells for these two cases are shown in Figures 2.2.c and 2.2.f and correspond to resulting structures where coating was correspondingly carried out before (pre) and after (post) the assemblying of the structure. The chosen metal and coating thickness (i.e., δ_m and δ_a) were 50 μm and 30 μm, respectively, using air as the medium. The results shown corresponds to runs 10, 21, 22 and 23 in Table 3.1. When the coating layer separated the metal foils from direct contact, the k_{eff} of the system in the case of using aluminum as the metal was calculated

to be 0.121 W/m/K, which is found to be only just 8% better than the conductivity calculated for the case where SS 304 is used as the metal. Though aluminum metal has a conductivity 16 times higher than that of SS 304, the k_{eff} of the bed was simply not affected by the type of metal used. In other words, the role of the metal is non existent when the metal of the foils are not in direct contact with each other. A contrastingly different result is observed when the metal between adjacent foils were in direct contact with each other. The k_{eff} of the system with SS 304 is 0.561 W/m/K, which has an increase by 5 times when compared to pre-assembly coated structures, and is similar to the value previously discussed in Figure 3.1. When aluminum metal was used, a massive increase in 55 times from the pre-assembly coating was observed with value 6.665 W/m/K. This clearly shows that a post assembly coating methodology significantly impacts the overall k_{eff} of the bed.

Figure 3.10 shows the scenario of having an even (as shown by Figure 2.3.a) and uneven (as shown by Figure 2.3.b) array of distribution of the SS 304 metal foils of 50 μm thickness, having 30 μm adsorbent coating with air as the medium, and using loose foils with point contact (δ_g = 0 μm). The unit cell used is that of Figure 2.2.c. The results here corresponds to the runs 10 and 24 in Table 3.1. The effective thermal conductivity of the system is found to be 0.113 W/m/K, which is identical to the run 10 value of 0.112 W/m/K. Therefore the alignment does not affect the conductivity of the system under study.

CONCLUSION

The thermal conductivity studies on the structured adsorbent system was studied using the simulation tool under various design conditions included the thickness of the

adsorbent coating, the thickness of the metal, the type of metal, loose or imbedded corners at the point of contact between corrugated and smooth foils, the presence and magnitude of air gap between the foils, coating on just one or both sides of the foils, the array of the cells and the role of the gas medium.

The results generally showed that direct metal-metal foil contact is the single most important design feature in designing thermally conductive bed. Under this condition, thermal conductivity depends strongly on the metal conductivity, and weakly on the gas medium and all other design properties. For these metal foils in air, the thermal conductivities varied between 0.561 and 0.629 W/m/K, when the metal was stainless steel, whereas for aluminum, a value of 6.66 W/m/K was obtained. In contrast, when the foils were separated either by air gaps or by a 13X coating, the effective thermal conductivity was significantly reduced, and it depended strongly on the gas medium but only and weakly on the metal conductivity and all other design properties. In air, whether the metal was stainless steel 304 or aluminum, the thermal conductivities were always around 0.090 and 0.125 W/m/K. These number represent about 80% reduction in conductivity in case of stainless steel 304 and more than 98% reduction in the case of aluminum.

As is it evident that the presence of either gas medium gaps or adsorbent between the foils could greatly impact the conductivity of the system, it becomes important while manufacturing to have a compact structure with no gaps in between while ensuring continuous metal to metal contact between metal foils. The result of having a much improved thermal conductivity with the post-assembly coating makes it an attractive methodology to be implemented in the manufacturing process for the application in TSA systems in order to overcome the slow heating problems.

Table 2.1: Variables investigated in this study.

Metal	Stainless steel AISI 304, Aluminum
Adsorbent	Zeolite 13X (With or without)
Gas medium	Air, He, CO_2
Coating	Pre or post assembly
Coating	Only on corrugated metal foil, Both foils
Foil configuration	Even or uneven
Foil assembly	Imbedded or loose
δ_a, μm	30, 50, 100
δ_m, μm	50, 80, 100
δ_g, μm	0, 10, 30, 50

Table 2.2: Properties of the materials.

Properties	**Stainless Steel AISI 304**	**Zeolite 13X**	**Aluminum**
Thermal Conductivity (k), W/m/K	14.90	0.15	238.00
Density (ρ) , kg/m^3	7,900.0	1,100.0	2,700.0

Table 3.1: A summary of the entire work with the different designs and simulation conditions used as a part of the modelling.

Run	Case in Fig. 2.2*	Array	Coat **	δ_a µm	δ_m µm	Metal	Contact	δ_g µm	Gas	w cm	k_{eff} W/m/K
1	a	Even	-	0	50	SS 304	Loose	0	Air	1.247	0.575
2	b	Even	-	0	50	SS 304	Imbed	-	Air	1.247	0.629
3	a	Even	-	0	50	SS 304	Loose	0	He	1.247	0.726
4	a	Even	-	0	50	SS 304	Loose	0	CO_2	1.247	0.563
5	a	Even	-	0	50	SS 304	Loose	10	Air	1.353	0.119
6	a	Even	-	0	50	SS 304	Loose	30	Air	1.375	0.099
7	a	Even	-	0	50	SS 304	Loose	50	Air	1.407	0.090
8	a	Even	-	0	50	SS 304	Loose	10	He	1.353	0.460
9	a	Even	-	0	50	SS 304	Loose	10	CO_2	1.353	0.085
10	c	Even	Pre	30	50	SS 304	Loose	0	Air	1.480	0.112
11	c	Even	Pre	30	50	SS 304	Loose	0	He	1.480	0.345
12	c	Even	Pre	30	50	SS 304	Loose	0	CO_2	1.480	0.087
13	c	Even	Pre	50	50	SS 304	Loose	0	Air	1.580	0.107
14	c	Even	Pre	100	50	SS 304	Loose	0	Air	1.827	0.101
15	d	Even	Post	30	50	SS 304	Imbed	-	Air	1.253	0.620
16	d	Even	Post	50	50	SS 304	Imbed	-	Air	1.257	0.623
17	d	Even	Post	100	50	SS 304	Imbed	-	Air	1.267	0.623
18	c	Even	Pre	30	80	SS 304	Loose	0	Air	1.550	0.120
19	c	Even	Pre	30	100	SS 304	Loose	0	Air	1.600	0.125
20	e	Even	Pre	30	50	SS 304	Loose	0	Air	1.426	0.118
21	c	Even	Pre	30	50	Al	Loose	0	Air	1.480	0.121
22	f	Even	Post	30	50	SS 304	Loose	0	Air	1.253	0.561
23	f	Even	Post	30	50	Al	Loose	0	Air	1.253	6.665
24	c	Uneven	Pre	30	50	SS 304	Loose	0	Air	1.480	0.113

$*$ D_{bed} is 0.32 cm for all the design cases under study.

** Pre-assembly (Pre) coating where the metal foils are first coated with adsorbent and then assembled. Post-assembly (Post) coating where the metal foils are first assembled together and then coated with adsorbent.

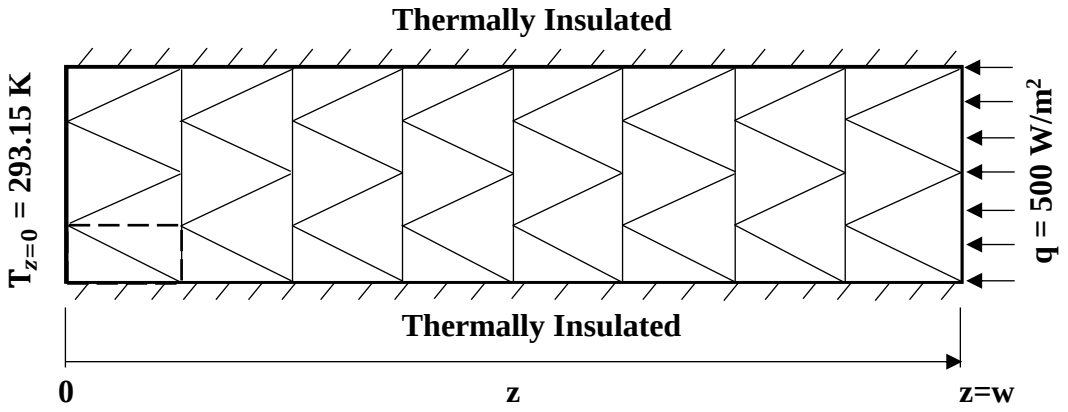

Figure 2.1**:** Control volume of the model using 8 layers of intercalated coated corrugated and 9 layers of smooth metal foils using a gas with the boundary conditions. The unit cell is highlighted at the bottom left corner of figure. Unit cells for each of the cases studied are magnified and represented in Figure 3.2.

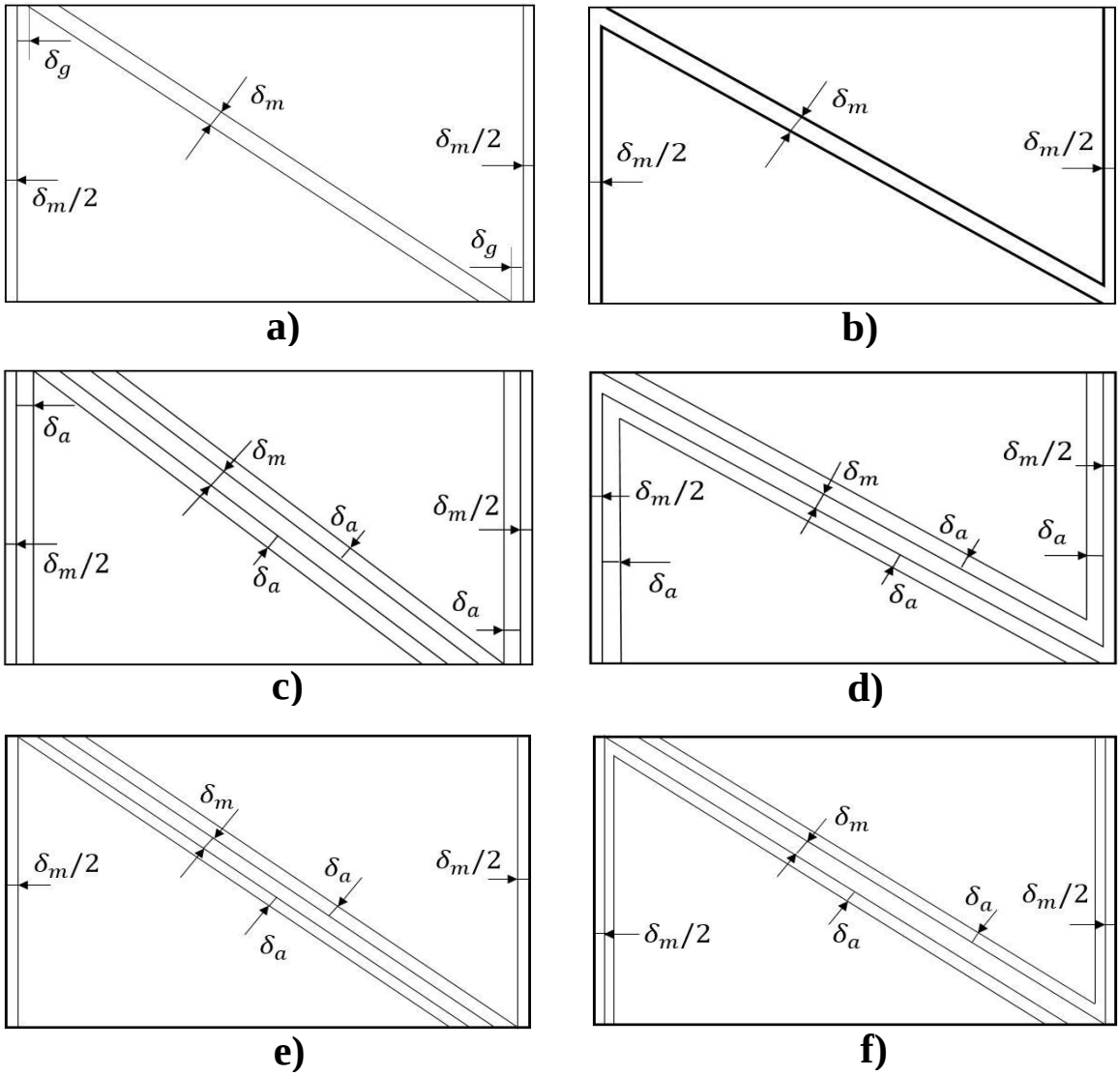

Figure 2.2: Representative case for a cell with intercalated smooth and corrugated metal foils a) loose contact foils of thickness δ_m with no adsorbent coating and gas gap δ_g; b) imbedded foils of thickness δ_m with no adsorbent coating; c) loose contact foils of thickness δ_m with adsorbent coating of thickness δ_a and no gas gap; d) imbedded foils of thickness δ_m with adsorbent coating of thickness δ_a; e) loose foils of thickness δ_m with adsorbent coating of thickness δ_a only on the corrugated foils and no gas gap; and f) loose foils of thickness δ_m with adsorbent coating of thickness δ_a with no gas gap but with metal foils in direct contact.

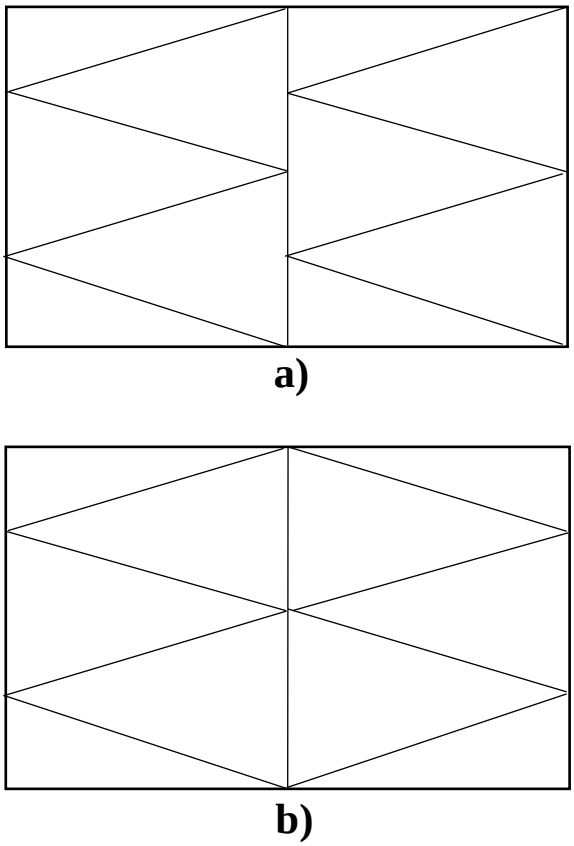

Figure 2.3: A representative array of a) even b) uneven distribution of the metal foils

Figure 3.1: Effect of the nature of contacts between the foils on the k_{eff} perpendicular to the structure bed layers with the bed containing loose foils with zero gap (Run 1) and imbedded foils (Run 2) having 50 μm foils with air as gas medium.

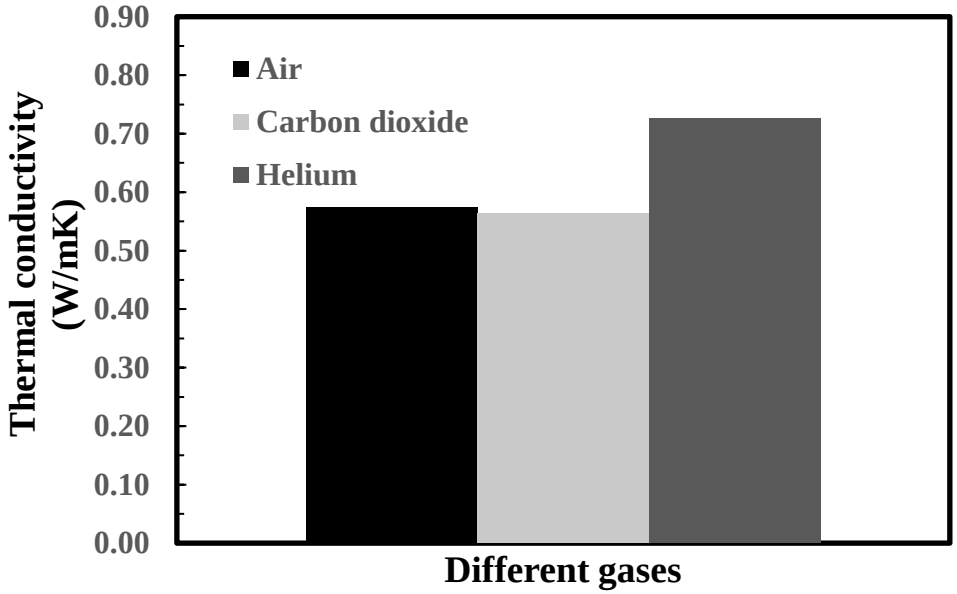

Figure 3.2: Effect of the different gas media (i.e., 1, 3, and 4) on the k_{eff} perpendicular to the structure bed layers with the bed containing loose metal foils in contact of 50 μm thickness.

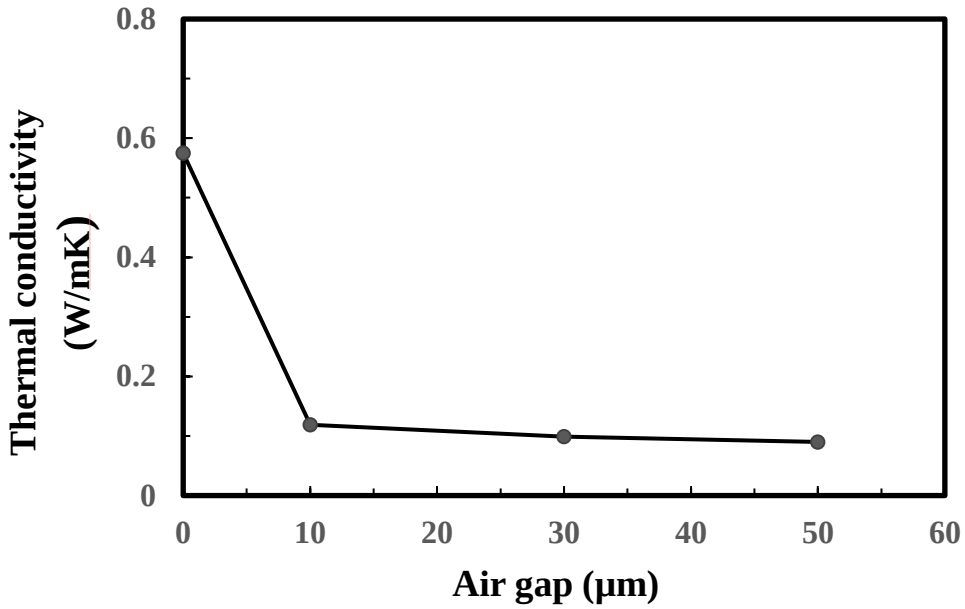

Figure 3.3: Effect of the air gaps δ_g between the smooth and corrugated foils on the k_{eff} perpendicular to the structure bed layers with the bed containing gaps of 0, 10, 30, 50 μm (i.e., runs 1, 5, 6 and 7) between the metal foils of 50 μm thickness.

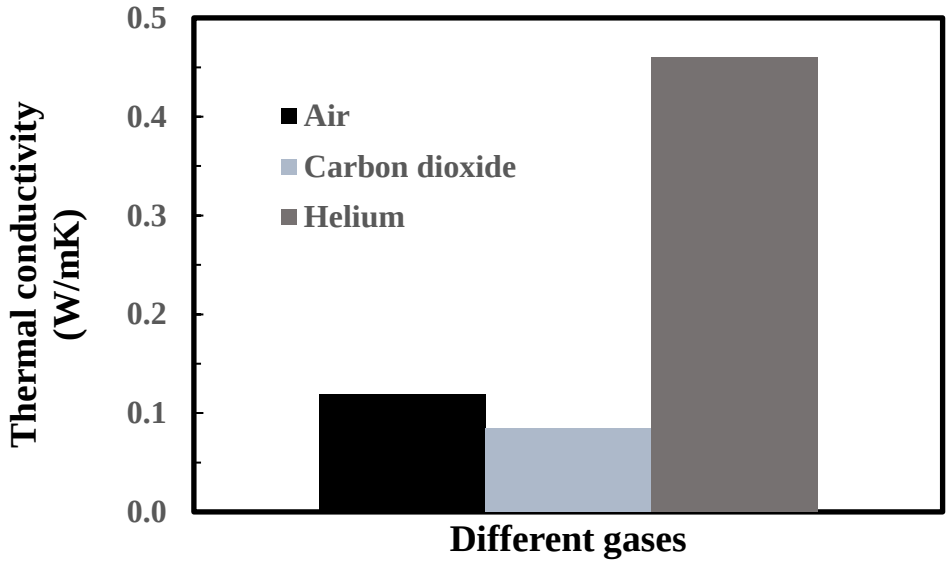

Figure 3.4: Effect of the different gas media on the k_{eff} perpendicular to the structure bed layers with the bed having 10 μm gap (i.e., runs 5, 8 and 9) between the metal foils of 50 μm thickness and no coating.

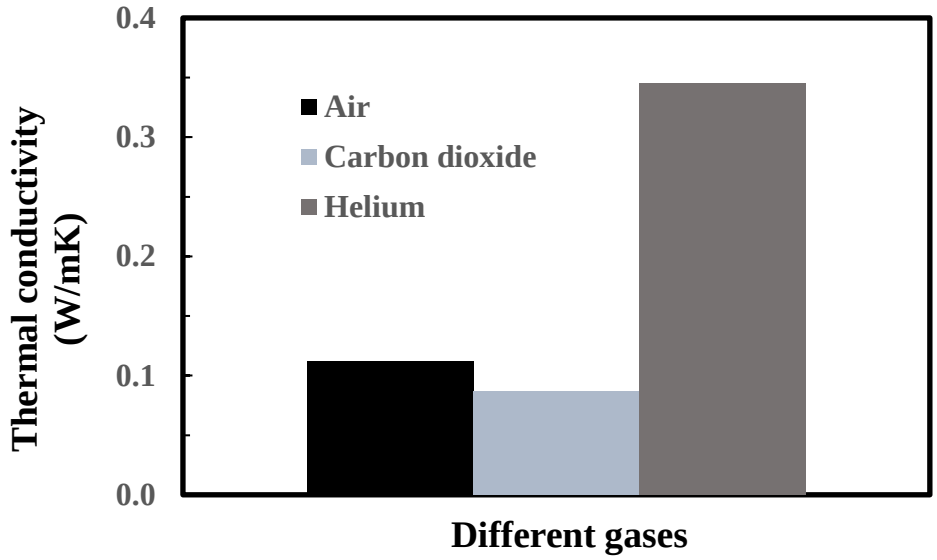

Figure 3.5: Effect of the different gas media (i.e., runs 10, 11 and 12) on the k_{eff} perpendicular to the structure bed layers with the bed containing metal foils of 50 μm in thickness with 30 μm coating thickness.

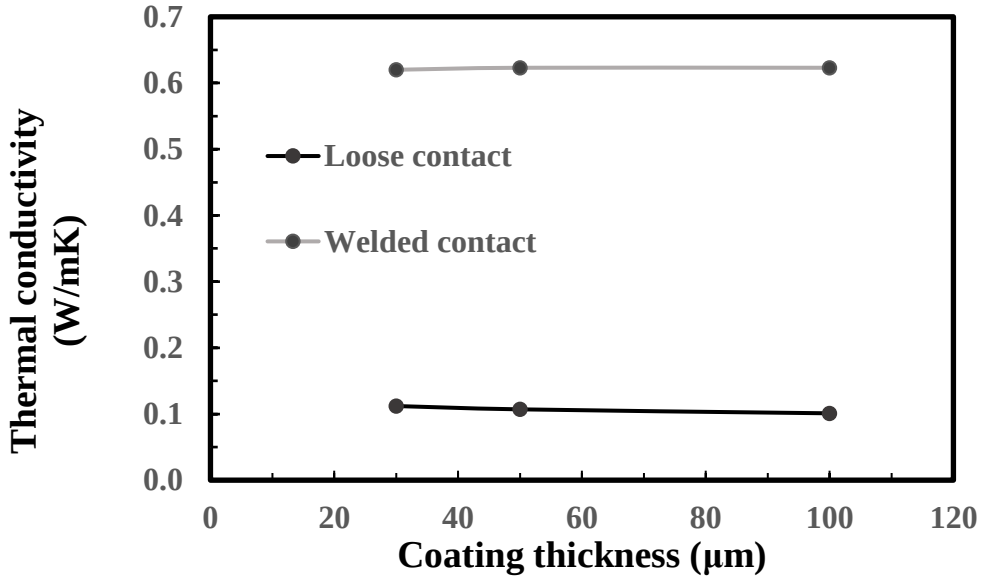

Figure 3.6: Effect of the thickness of adsorbent coating δ_a of 30, 50 and 100 μm on the k_{eff} perpendicular to the structure bed layers on both the metal foils of 50 μm thickness having loose (i.e., runs 10, 13 and 14) and imbedded contacts (i.e., runs 15, 16 and 17) between them with air as the medium.

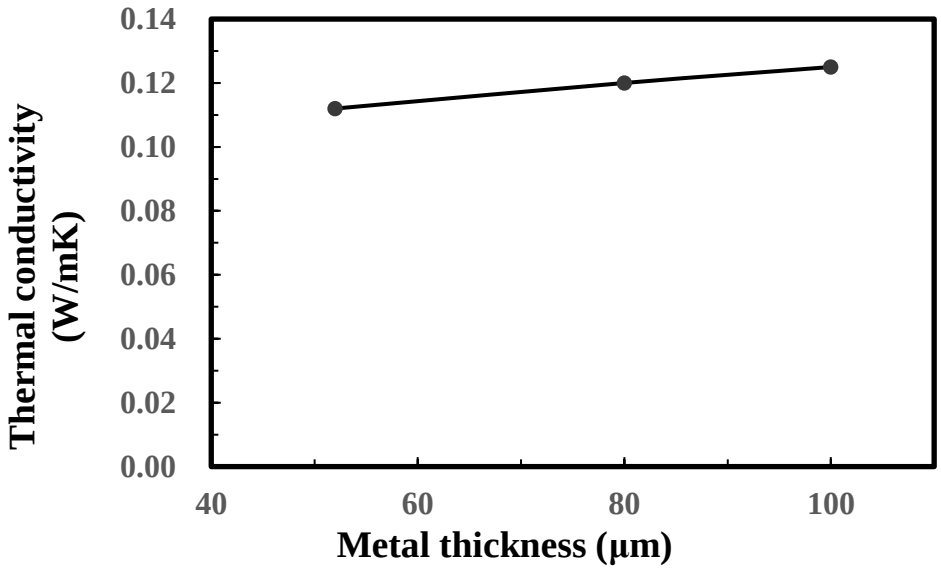

Figure 3.7: Effect of the metal thickness δ_m on the k_{eff} perpendicular to the structure bed layers with the bed containing metal foils of 50, 80 and 100 μm in thickness (i.e., runs 10, 18 and 19) with 30 μm coating thickness with air as the medium.

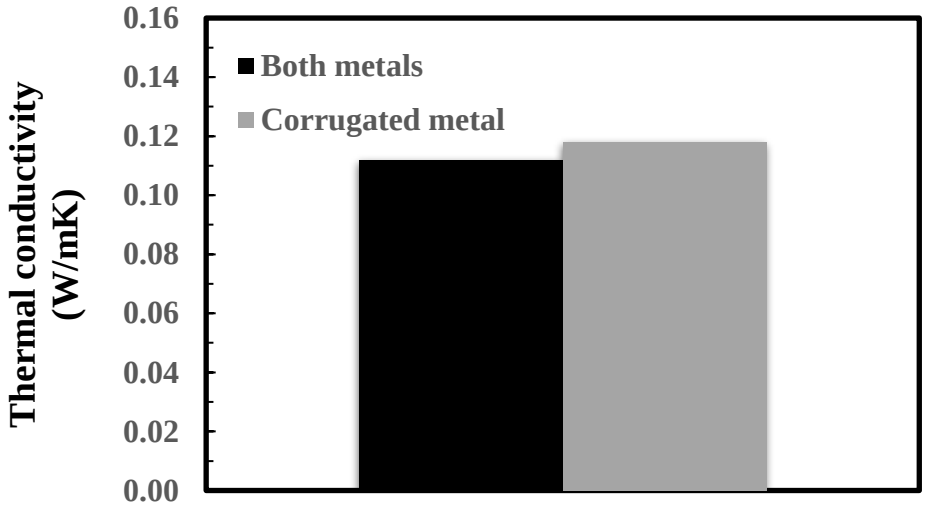

Figure 3.8: Effect of having pre-assembly adsorbent coating of 30 μm in thickness on both the metal foils (i.e., run 10) and only on the corrugated metal foils (i.e., run 20) of 50 μm in thickness with air as the medium.

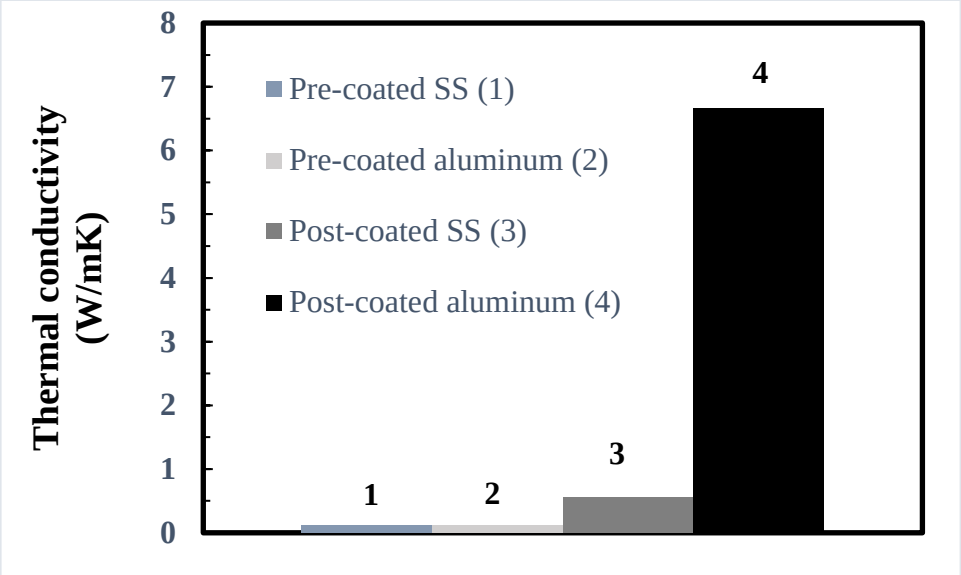

Figure 3.9: Effect of using different metals for the foils of structure bed layers on the k_{eff} with the bed containing 50 μm in thickness foils with pre-assembly 30 μm coating (i.e., runs 10, and 21) and post- assembly 30 μm coating (i.e., runs 22, and 23) with air as the medium.

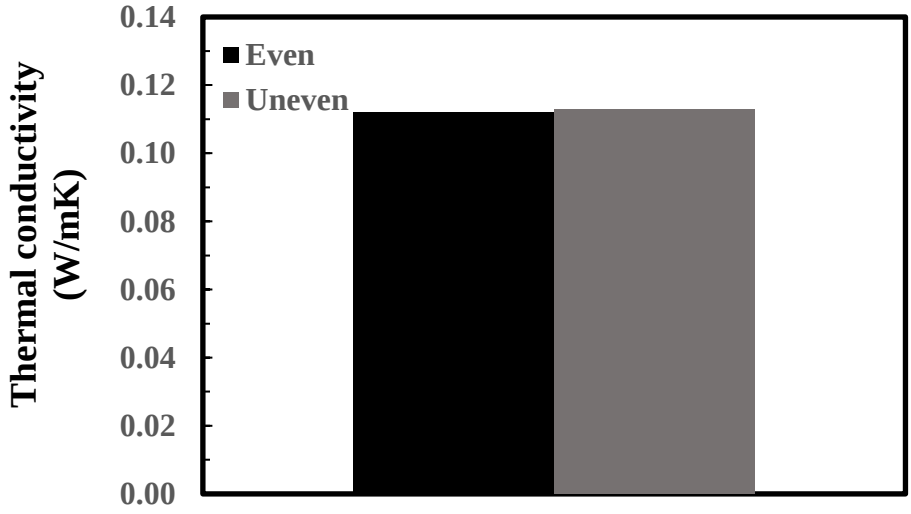

Figure 3.10: Effect of the alignment on the k_{eff} perpendicular to the structure bed layers with the bed containing metal foils of 50 μm in thickness (i.e., runs 10, and 24) having 30 μm coating with air as the medium.

REFERENCES

1) "Adsorption, Gas separation", Kirk-Othmer Encyclopedia of Chemical Technology, Vol. 1.

2) Rezaei, F.; and Webley, P., "Structured adsorbents in gas separation processes", *Separation and Purification Technology* **70**, 243–256 (2010).

3) Rezaei, F.; Mosca, A.; Webley, P.; Hedlund, J.; and Xiao, P., "Comparison of Traditional and Structured Adsorbents for CO_2 Separation by Vacuum-Swing Adsorption", *Ind. Eng. Chem. Res.* **49**, 4832–4841 (2010).

4) Bailey, A.; Maggs, F.A.P., US Patent US4, 234,326 (1980).

5) Golden, T.C.; Golden C.M.A.; and Zwilling, D.P., US Patent US6, 565,627 (2003).

6) Sawad, J.A.; Alizadeh-Khiavi, S.; Roy, S.; and Kuznicki, S.M., W.I.P.O. Patent WO2005032694 (2005).

7) Petkovska, M.; Tondeur, D.; Grevillot, G.; Granger, J.; and Mitrovic, M., "Temperature-Swing Gas Separation with Electrothermal Desorption Step", *Sep. Sci. Technol.* **26** 425–444 (1991).

8) Sullivan, P.D.; Rood, M.J.; Hay, K.J.; and Qi, S., "Adsorption and Electrothermal Desorption of Hazardous Organic Vapors", *J. Environ. Eng.* **127**, 217–223 (2001).

9) Patcas, F.C.; Garrido, G.I.; and Kraushaar-Czarnetzki, B., "CO oxidation over Structured Carriers: A comparison of Ceramic Foams, Honeycombs and Beads", *Chem. Eng. Sci.* **62,** 3984–3990 (2007).

10) Yoon, K.B.; Lee, Y.J.; Park, Y.S.; and Lee, J.S., US Patent US2, 002,183,407 (2002).

11) Keefer, B.G., US Patent US5, 082,473 (1992).

12) Keefer, B.G., US Patent US6, 176,897 (2001).

13) Maurer, R.T., US Patent US5, 338,450 (1994).

14) Keefer, B.G.; Carel, A.; Sellars, B.; Shaw, I.; and Larisch, B., US Patent, US6, 692,626 (2004)

15) Kodama, A.; Goto, M.; Hirose, T.; et al., "Parametric Studies of a Silica Gel Honeycomb Rotor Adsorber Operated with Thermal Swing," *J. Chem. Eng. Jap.* **29** (1996).

16) Kodama, A.; Goto, M.; Hirose, T.; et al., "Performance Evaluation for Thermal Swing Honeycomb Rotor Adsorber Using a Humidity Chart," *J. Chem. Eng. Jap.* **28**, 19-24 (1995).

17) Kodama, A.; Goto, M.; Hirose, T.; et al., "Temperature Profile and Optimal Rotation Speed of a honeycomb Rotor Adsorber Operated with Thermal Swing," *J. Chem. Eng. Jap.* **27**, 644-649 (1994).

18) Kodama, A.; Goto, M.; Hirose, T.; et al., "Experimental Study of Optimal Operation for a Honeycomb Adsorber Operated with Thermal Swing," *J. Chem. Eng. Jap.* **26**, 530-535 (1993).

19) Chang, F.T.; Lin, Y.C.; Bai, H.; et al., "Adsorption and desorption characteristics of Semiconductor Volatile Organic compounds on the Thermal Swing Honeycomb Zeolite Concentrator," *Air & Waste Manage. Assoc.* **53**, 1384-1390 (2003).

20) Yamauchi, H.; Kodama A.; Hirose T.; et al., "Performance of VOC Abatement by Thermal Swing Honeycomb Rotor Adsorbers," *Ind. Eng. Chem. Res.* **46**, 4316-4322 (2007).

21) Kondakindi, R.R.; McCumber, G.; Aleksic, S.; Whittenberger, W.; and Abraham, M.A., "Na_2 CO_3-based Sorbents Coated on Metal foil: CO_2 Capture Performance", *Int. J. Greenh. Gas Control* **15,** 65–69 (2013).

22) Menard, D.; Py, X.; Mazet, N., "Activated Carbon Monolith of High Thermal Conductivity for Adsorption Processes improvement Part A. Adsorption step," *Chem. Eng. and Process.* **44**, 1029-1038 (2005).

23) Menard, D.; Py, X.; and Mazet, N., "Activated Carbon Monolith of High Thermal Conductivity for Adsorption Processes improvement Part B. Thermal regeneration," *Chem. Eng. Process.* **46**, 565-572 (2007).

24) Grande, C. A.; Cavenati, S.; Barcia P.; et al., "Adsorption of Propane and Propylene in Zeolite 4A Honeycomb Monolith," *Chem. Eng. Sci.* **61**, 3053-3067 (2006).

25) Ribeiro, R. P.; Sauer, T. P.; Lopes, F. V.; et al., "Adsorption of CO_2, CH_4 and N_2 in Activated Carbon Honeycomb Monolith," *J. Chem. Eng. Data* **53**, 2311-2317 (2008).

26) Yates, M.; Blanco, J.; Avila, P.; and Martin, M.P., "Honeycomb Monoliths of Activated Carbon for Effluent Gas Purification", *Micropor. Mesopor. Mater.* **37,** 201–208 (2000).

27) Gorbach, A.B.; Stegmaier, M.; Eigenberger, G.; Hammer, J., and Fritz, H.G., "Compact Pressure Swing Adsorption Processes-Impact and Potential of New-Type Adsorbent-Polymer Monoliths", *Adsorption* **11**, 515–520 (2005).

28) Yu, F.D.; Luo, L.A.; and Grevillot, G., "Adsorption Isotherms of VOCs onto an Activated Carbon Monolith: Experimental Measurement and Correlation with Different Models", *J. Chem. Eng. Data* **47,** 467–473 (2002).

29) Yu, F.D.; Luo, L.A.; and Grevillot, G., "Electrothermal Desorption using Joule Effect on an Activated Carbon Monolith", *J. Environ. Eng*. **130,** 242–248 (2004).

30) Gadkaree, K.P., **"**Carbon Honeycomb Structures for Adsorption applications", *Carbon* **36,** 981–989 (1998).

31) Mosca, A.; Hedlund, J.; Ridha, F.N.; Webley, P., "Optimization of Synthesis procedures for Structured PSA adsorbents", *Adsorption* **14,** 687-693 (2008).

32) Valdes-Solis, T.; Linders, M.J.G.; Kapteijn, F.; Marban, G.: and Fuertes, A.B., "Adsorption and Breakthrough performance of Carbon-coated Ceramic Monoliths at Low Concentration of n-butane", *Chem. Eng. Sci*. **59**, 2791–2800 (2004).

33) Ohrman, O.; Hedlund, J.; and Sterte, J., "Synthesis and evaluation of ZSM-5 films on Cordierite Monoliths", *Appl. Catal. A: Gen*. **270,** 193–199 (2004).

34) Mosca, A.; Hedlund, J.; Webley. P.; Grahn, M.; and Rezaei, F., "Structured zeolite NaX coatings on Ceramic Cordierite Monolith Supports for PSA applications", *Micropor. Mesopor. Mater*. **130**, 38-48 (2010).

35) Belding, W.A.; Delmast, M.P.F.; and Holeman, W.D., "Desiccant Aging and Its Effects on Desiccant Cooling System Performance" *Applied Thermal Engineering* Vol. **16**, No. 5. 447-459. (1996).

36) Belding, W.A.; and Delmas, M.P.F., “Novel Desiccant Cooling system using Indirect Evaporative Cooler” *ASHRAE Transactions*, vol. **103**, part 1, 841-847 (1997).

37) Belding, W.A.; Worek, W.M.; and Novosel, D., “Desiccant development for Gas-fired Desiccant Cooling systems” *ASHRAE Transactions* **97**(1), 587-94 (1991).

38) Incropera, F.P.; Dewitt, D.P.; Bergman, T.L.; and Lavine, A.S., “Introduction to Heat Transfer”, Fifth edition, John Wiley & Sons, Inc. (2007).